Lattice dynamics and thermal properties of thorium metal and thorium monocarbide

L. Kývala[1,2] and D. Legut[2]

[1]*Nanotechnology Centre, VSB-Technical University of Ostrava, 17. listopadu 2172/15, 708 00 Ostrava, Czech Republic*

[2]*IT4Innovations, VSB-Technical University of Ostrava, 17. listopadu 2172/15, 708 00 Ostrava, Czech Republic*

(Received 10 May 2019; revised manuscript received 13 January 2020; accepted 22 January 2020; published 18 February 2020)

Thorium is a chemical element that is beginning to attract attention because of its potential use as a nuclear fuel. It is not easy to carry out experiments because of its radioactive nature, and therefore theoretical works are highly appreciated. Thorium contains only a small number of the $5f$ states, and it is generally accepted that these states are itinerant, that they form a chemical bond, and that their nature does not need to be corrected with the Hubbard model. On the other hand, there is a well-known problem with the description of the $6p_{1/2}$ states when the spin-orbit coupling is added as the perturbation to a scalar-relativistic calculation. Electronic, elastic, phonon, and thermodynamic properties are analyzed in terms of the importance of the spin-orbit coupling acting on the $6d$ and $5f$ states. The importance of the spin-orbit coupling acting on the semicore $6p$ states is discussed. The same properties are analyzed for thorium monocarbide, and a difference caused by adding a carbon atom into the structure is discussed. Detailed analysis of the thermal conductivity (both phonon and electronic contributions) is also included. We have given extra attention to the thermal conductivity of ThC to explain why the optical phonon modes account only for approximately 6% of the phonon thermal conductivity.

DOI: 10.1103/PhysRevB.101.075117

I. INTRODUCTION

Thorium (Th), the second actinide element, is a weakly radioactive silvery metal with atomic number 90. Thorium metal possesses the face-centered cubic (fcc) structure (space group $Fm\bar{3}m$, No. 225) at ambient conditions and exhibits only Pauli paramagnetism [1] due to *f-f* states overlapping [2].

From the thorium position in the periodic table, one could assume that thorium metal should possess the hexagonal close-packed (hcp) crystal structure as other elements in group IVA elements (Ti, Zr, and Hf). However, among these tetravalent elements, thorium is the only one that holds the fcc crystal structure. It is believed to be attributed to the presence of the $5f$ states involved in chemical bonds [3]. Without occupation of the $5f$ states, thorium would hold the body-centered cubic (bcc) crystal structure and would exhibit normal tetravalent d metal behavior as in the case of Ti, Zr, and Hf [3]. Only when the $5f$ state occupation is taken into account does the fcc structure become the ground-state structure in agreement with experiments.

Typical applications of thorium compounds include incandescent gas mantles, production of ceramics, carbon arc lamps, coatings for tungsten welding rods, refractive glass additives, and heat-resistant laboratory crucibles, and Th can also be used as a catalyst [4]. However, current attention paid to this element is due to possible use as a nuclear fuel in generation IV nuclear reactors [5]. Thorium is 3 to 4 times more abundant than uranium while widely distributed in nature as an easily exploitable resource in many countries. Unlike uranium where it is necessary to distinguish the "fissile" ^{235}U isotope and ^{233}U isotope, thorium can be found only in the "fertile" ^{232}Th isotope. Moreover, the thorium fuel cycle produces less radiotoxic waste than the uranium fuel cycle [6].

Thorium monocarbide is one of the possible compounds that could be used in nuclear power engineering. The material properties of carbide are significantly different from its metal. Although it retains space group $Fm\bar{3}m$ (No. 225) at ambient conditions, a significant part of bonding in light actinide monocarbides forms ionic bonds due to considerable electronegativity difference between actinide and carbon. Nevertheless, thorium monocarbide keeps its metallic behavior, and therefore more attractive thermodynamic properties for nuclear energy can be expected thanks to conductive electrons in comparison to isolating oxides. Because of the well-known hybridization of the actinide $6d$, $5f$, and carbon $6p$ orbitals, the covalent part of bonding is included as well. As far as magnetism is concerned, thorium monocarbide is paramagnetic [7].

In this work, employing density functional theory (DFT) electronic structure calculations, we investigate physical aspects affecting elastic, phonon, and thermodynamic properties of thorium metal and its monocarbide. We investigate separately the effect of taking into account the spin-orbit coupling on valence $6d$ and $5f$ states, and whether the scalar-relativistic base of the semicore $6p$ states is sufficient.

The thermal conductivity analysis is one of the main concerns here as the heat transfer belongs among the fundamental properties for nuclear fuel material design.

II. THEORETICAL METHODOLOGY

In the harmonic approximation, crystal potential energy ϕ is expanded as

$$\phi = \phi_0 + \sum_{lk}\sum_{\alpha}\phi_\alpha(lk)u_\alpha(lk) + \frac{1}{2}\sum_{ll'kk'}\sum_{\alpha\beta}\phi_{\alpha\beta}(lk,l'k')u_\alpha(l'k'), \tag{1}$$

where l and k are the labels of unit cells and atoms in each unit cell, α and β are the Cartesian indices, and ϕ_0, $\phi_\alpha(lk)$, $\phi_{\alpha\beta}(lk, l'k')$ are the zeroth-, first-, and second-order force constants.

An element of second-order force constant $\phi_{\alpha\beta}(lk, l'k')$ is obtained from a force $F_\alpha(lk)$:

$$\frac{\partial^2\phi}{\partial u_\alpha(lk)\partial u_\beta(l'k')} = -\frac{F_\beta(l'k')}{\partial u_\alpha(lk)}. \tag{2}$$

The Helmholtz free energy F from the canonic distribution for phonons under the harmonic approximation is given as

$$F_{\mathrm{ph}}(T, V) = \frac{1}{2}\sum_{\boldsymbol{q}\nu}\hbar\omega_{\boldsymbol{q}\nu} + k_B T\sum_{\boldsymbol{q}\nu}\ln\left[1 - \exp\left(-\frac{\hbar\omega_{\boldsymbol{q}\nu}}{k_B T}\right)\right], \tag{3}$$

where $\boldsymbol{q}$ is the wave vector and ν is the band index.

Phonon properties vary with changes of volume because a crystal potential is an anharmonic function of volume. However, it is possible to calculate thermodynamic properties in agreement with experiments from the harmonic potential if a temperature is well below a melting point.

Thermodynamic properties are calculated in the so-called quasiharmonic approximation. The harmonic approximation at each volume is applied and the volume dependence on temperature is achieved by minimizing the Gibbs free energy (G) at a given temperature and pressure,

$$G(T, p) = \min_V[F(T, V) + pV], \tag{4}$$

where the minimum value in the square bracket is found by changing volume (V). The Helmholtz free energy $F(T, V)$ consists of the internal energy $U(V)$ which is obtained as the total energy of electronic structure from first-principles calculations and $F_{\mathrm{ph}}(T, V)$ from Eq. (3). Subsequently, thermodynamic quantities are calculated from this free energy at constant pressure.

The lattice thermal conductivity (κ) can be obtained from the solution of the Boltzmann transport equation. Although the full solution of the linearized phonon Boltzmann equation exists (details in Ref. [8]), the thermal conductivity (κ) is more often calculated using the relaxation time approximation (RTA), which is much simpler and gives the same results in most cases [8]. The lattice thermal conductivity (κ) within the relaxation time approximation is given by

$$\kappa^{\mathrm{RTA}} = \frac{1}{NV_0}\sum_{\boldsymbol{q}\nu} C_{\boldsymbol{q}\nu} v_{\boldsymbol{q}\nu} \otimes v_{\boldsymbol{q}\nu}\tau^{\mathrm{RTA}}_{\boldsymbol{q}\nu}, \tag{5}$$

where V_0 is the volume of a unit cell, and $C_{\boldsymbol{q}\nu}$, $v_{\boldsymbol{q}\nu}$, $\tau_{\boldsymbol{q}\nu}$ are the heat capacity, group velocity, and phonon lifetime of the phonon mode at the wave vector ($\boldsymbol{q}$) and phonon mode (ν).

The phonon mode lifetime $\tau_{\boldsymbol{q}\nu}$ is reciprocal to the phonon linewidth $\Gamma_{\boldsymbol{q}\nu}(\omega_{\boldsymbol{q}\nu})$,

$$\tau_{q\nu} = \frac{1}{2\Gamma_{\boldsymbol{q}\nu}(\omega_{\boldsymbol{q}\nu})}, \tag{6}$$

where the phonon linewidth ($\Gamma_{\boldsymbol{q}\nu}$) is determined from the three-phonon scattering using the many-body perturbation theory [8].

Transport coefficients are calculated within the rigid-band approximation, which assumes that the band structures do not change by changing the temperature, or by doping [9]. It allows us to calculate the carrier concentration for a given T and μ directly from the density of states (DOS),

$$n(\epsilon) = \int\sum_b \delta(\epsilon - \epsilon_{b,\boldsymbol{k}})\frac{d\boldsymbol{k}}{8\pi^2}, \tag{7}$$

where the subscript b runs over bands, by calculating the deviation from charge neutrality

$$c(\mu, T) = N - \int n(\epsilon) f^{(0)}(\epsilon; \mu, T) d\epsilon. \tag{8}$$

The parameter N stands for the nuclear charge and $f^{(0)}$ is the Fermi distribution function.

The Boltzmann transport equation (BTE) for electrons describes a balance between scattering in and out of each possible state with scalar scattering rates [10]. The transport distribution function of the linearized version of the BTE under the RTA,

$$\sigma(\epsilon, T) = \int\sum_b \boldsymbol{v}_{b\boldsymbol{k}} \otimes \boldsymbol{v}_{b\boldsymbol{k}}\tau_{b\boldsymbol{k}}\delta(\epsilon - \epsilon_{b,\boldsymbol{k}})\frac{d\boldsymbol{k}}{8\pi^2}, \tag{9}$$

is used to calculate the moments of the generalized transport coefficient,

$$\mathcal{L}^{(\alpha)}(\mu; T) = q^2\int\sigma(\epsilon, T)(\epsilon - \mu)^\alpha\left(-\frac{\partial f^{(0)}(\epsilon; \mu, T)}{\partial\epsilon}\right)d\epsilon. \tag{10}$$

For zero temperature gradient and zero electric current, the electrical conductivity σ and the electron thermal conductivity κ_e can be calculated as

$$\sigma = \mathcal{L}^{(0)}, \tag{11}$$

$$\kappa_e = \frac{1}{q^2 T}\left[\frac{(\mathcal{L}^{(1)})^2}{\mathcal{L}^{(0)}} - \mathcal{L}^{(2)}\right]. \tag{12}$$

However, both quantities are dependent on the relaxation time of electrons τ. It cannot be derived from this approach because it comes from the electron-phonon interactions.

We use the Sommerfeld approximation to calculate the entropy of electrons [11]:

$$S_{\mathrm{el}} = \frac{\pi^2}{3}k_B^2\, T\, n(E_F), \tag{13}$$

where $n(E_F)$ is the number of states at the Fermi energy. Then the Sommerfeld coefficient can be easily derived from the electronic entropy:

$$\gamma = \frac{dS}{dT} = \frac{\pi^2}{3}k_B^2\, n(E_F). \tag{14}$$

The Debye temperature is obtained by fitting

$$D(\omega) = a\omega^2 \tag{15}$$

to a frequency cutoff where the phonon DOS still has a harmonic shape. The frequency cutoff is not unique, and therefore this determination is not unambiguous. Then the Debye frequency is calculated from the parameter a as

$$\omega_D = \left(\frac{9N}{a}\right)^{1/3}. \tag{16}$$

III. COMPUTATIONAL DETAILS

Our DFT calculations in this study were carried out using the Vienna *Ab initio* Simulation Package (VASP) [12] with the projector augmented wave scheme (PAW) [13,14]. Electron exchange and correlation potentials were treated within the generalized gradient approximation of Perdew-Burke-Ernzerhof (GGA-PBE) [15] as well as with its revised version, the so-called PBEsol [16]. Valence electrons for thorium are in the $6s^2\,6p^6\,6d^1\,7s^2\,5f^1$ shells and the $2s^2\,2p^2$ configuration for carbon.

The kinetic energy cutoff for the plane-wave basis functions is 500 eV. Brillouin zone integrations were carried out using a $16 \times 16 \times 16\Gamma$-centered k-point mesh for fcc thorium and $12 \times 12 \times 12\,\Gamma$-centered k-point mesh for thorium monocarbide. We include the spin-orbit coupling (SOC) and apply the Hubbard model in the rotationally invariant approach [17] with $J = 0.4\,\text{eV}$ calculated from empirical rule $J = 0.33 + 0.070(Z - 89)$ [18] to thorium $5f$ states. The $4 \times 4 \times 4$ supercells containing 64 atoms with the $6 \times 6 \times 6\,\Gamma$-centered k-point mesh for fcc thorium and the $2 \times 2 \times 2$ supercells containing 64 atoms with the $4 \times 4 \times 4\,\Gamma$-centered k-point mesh for NaCl-type thorium monocarbide were used to calculate vibrational properties using the direct force-constant method as implemented in the PHONOPY [19] code and were used to calculate the phonon thermal conductivity by solving the Boltzmann transport equation within the RTA for phonons iteratively through third-order interatomic force constants based on the small-displacement method using PHONO3PY [8]. Electron transport coefficients were calculated by the semiclassical Boltzmann theory as implemented in the code BoltzTraP2 [9] from 50 000 irreducible k points in the unit cell. The convergence criteria for the system total energy and residual Hellmann-Feynman forces are set to $10^{-7}\,\text{eV}$ and $10^{-6}\,\text{eV/Å}$, respectively. Bulk moduli were obtained from fits to Vinet's equation of state [20]. The components of the elastic tensor are derived from the strain-stress relationship [21].

IV. RESULTS AND DISCUSSION

A. Electronic structure of thorium metal

Precise determination of the electronic structure is crucial for the accurate and realistic description of the lattice dynamics. Therefore, we thoroughly analyze the effect of the SOC on the electronic structure of thorium.

First, we present a modification of the electronic structure upon the SOC applied to only the $6d$ and $5f$ states in Fig. 1. It is difficult to find a difference between the scalar relativistic solution and the solution with the SOC included for the $6d$ and $5f$ electrons, not the $6p$. Only a slight change in the lattice parameter from 5.0523 Å to 5.0522 Å confirms that the $6d$ and $5f$ states are not affected by the SOC in this system.

If we apply the SOC to all electrons, including the $6p$, the vicinity of the Fermi energy does not seem to be changed as well. On the other hand, the $6p$ states are split into well-separated $6p_{1/2}$ and $6p_{3/2}$ states by about 6 eV. However, the $6p_{1/2}$ states are not described correctly because scalar relativistic p states are zero at the origin, but fully relativistic Dirac $6p_{1/2}$ states are not. So it is impossible to represent $p_{1/2}$ states with a linear combination of scalar relativistic

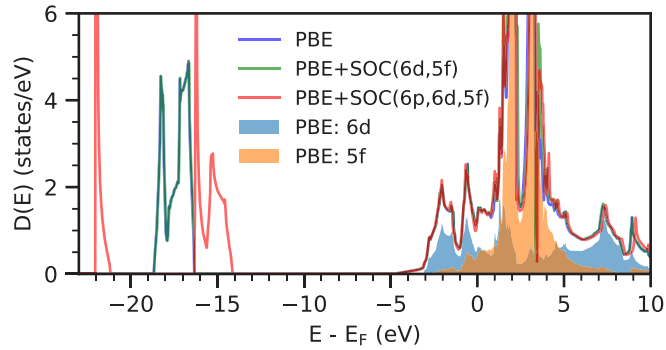

FIG. 1. The total densities of electron states $D(E)$ for fcc Th with the SOC neglected and included. The filled lines represent the $6d$ and $5f$ states of the PBE model.

basis functions. This problem occurs if the second variational approach is used. In the second variational approach, the scalar relativistic Hamiltonian is diagonalized first, and then given scalar eigenvectors and eigenvalues are used as a limited basis set for diagonalizing the full Hamiltonian including the spin-orbit coupling [22–24].

Mattsson and Wills [24] compare the second variational approach with the Dirac solution. They observe the shift of the $6p_{1/2}$ states to lower energy and as a result, the increase of $6p_{1/2} - 6p_{3/2}$ splitting around 1.3 eV. This result is consistent with the Kuneš *et al.* [23] approach, where they included additional local orbitals to mimic the correct behavior of relativistic p states within full potential linearized augmented plane wave methodology (FPLAPW).

Nevertheless, these two approaches are not consistent concerning the equilibrium volumes. Both predict the equilibrium volume reduction for the second variational approach but differ in assuming the equilibrium volume with the $6p_{1/2}$ state corrected base. Mattsson and Wills [24] report an increase in the volume of 0.3%, but Kuneš *et al.* [23] report a reduction of around 1%. The Dirac solution should be more precise in principle, but they use the atomic-sphere approximation, which is less accurate than the FPLAPW.

The second variational approach, which we use in this work, reduces the equilibrium volume around 1.6%. Next, we discuss what impact this reduction has and whether it improves compliance with experiments or vice versa.

A comparison of the Sommerfeld coefficients (listed in Table I) between PBE, PBE + SOC $(6d, 5f)$, or PBE + SOC $(6p, 6d, 5f)$ confirms that the electronic density does not change significantly near the Fermi energy (E_F). Nevertheless, the density of states with the inclusion of the SOC gives a better result when compared to the experimental measurements [25,26].

There is a 10% lower value of the Sommerfeld coefficient for the SOC$(6p, 6d, 5f)$ and the smaller electron-phonon coupling parameter ($\lambda = 0.456$) [27] with the SOC scheme in comparison with the scalar-relativistic scheme ($\lambda = 0.577$) [27]. Both are consistent with other calculations [28,29]. There is negligible difference between PBE and PBE + SOC$(6d, 5f)$ without the electron-phonon enhancement.

The density of states accuracy can be checked with BIS and XPS measurements [30]. Figure 2 shows that our result of

TABLE I. The calculated and experimental lattice parameters (a), elastic constants c_{ij}, bulk modulus B, Sommerfeld coefficient γ, and Debye temperatures θ_D of fcc Th.

	E_{xc}	U_{eff} (eV)	a (Å)	c_{11} (GPa)	c_{12} (GPa)	c_{44} (GPa)	B (GPa)	γ (mJ K^{-2} mol^{-1})	θ_D (K)	Reference
VASP	PBE	0.0	5.052	76.3	43.4	51.3	53.2	5.12	182	This work
	PBE + SOC($6d, 5f$)	0.0	5.052	76.0	43.4	50.9	53.5	4.73	181	This work
	PBE + SOC($6p, 6d, 5f$)	0.0	5.024	81.8	45.4	54.6	57.7	4.27	181	This work
	PBEsol + SOC($6p, 6d, 5f$)	4.0	5.069	75.9	59.8	40.1	63.8	4.02	151	This work
FP-LMTO			4.910	55	35	46	63			Söderlind [34,35]
ABINIT	PBE	0.0	5.024	84	40	58	55			Bouchet [36]
WIEN2K	PBE	0.0	5.062	76	41	53	57			Gupta [37]
Model potential				78	62	40	68			Baria [38]
VASP	PBE	0.0	5.062	81	41	49	50			Hu [39]
WIEN2K	PBE	0.0	5.080	76	44	44	55			Jaroszewicz [40]
Exp.			5.085	81	50	50	60			Greiner [32]
Exp.			5.089	78	48	51	58			Armstrong [33]
Exp.								4.23	167	Schmidt [25]
Exp.								4.31	163	Gordon [26]

PBE + SOC($6p, 6d, 5f$) agrees with the XPS experiment but fails with the BIS experiment.

We also calculated the DOS of Th with the PBEsol exchange-correlation approximation to try to reproduce the BIS experiment. However, the spectrum is very similar to the one obtained using the PBE approximation (Fig. 1, and Fig. S1 of the Supplemental Material [31]). The calculated lattice parameter of PBEsol 4.958 Å is lower than the experimental one 5.085 Å [32]. We applied the Hubbard U ($5f$ states) to increase the lattice parameter closer to the experimental value; its evolution is shown in Fig. S3. The value of 4 eV is needed for the agreement with experiments [32,33].

Figure S2 shows how the DOS evolves with the increasing value of the Hubbard U. The vicinity of the Fermi energy remains the same, but $5f$ states are moved to higher energies and $6p$ states are indirectly shifted to lower energies.

If we take the model which reproduces the experimental lattice constant (($U_{\text{eff}} = 4$ eV), we find consistency between such DOS and the XPS and even BIS experiment (Fig. 2).

The high value of the Hubbard U parameter acting on the $5f$ states is needed for the correct description of states lying high above the Fermi energy (E_F) of thorium, which is consistent with localized behavior of the $5f$ states in heavier actinides.

One has to keep in mind that such strong localization of the $5f$ states often has no physical meaning because there is approximately only one $5f$ electron which cannot be correlated. The PBEsol exchange and correlation potential should be used only for calculation of optical properties and other quantities related to the high-energy bands.

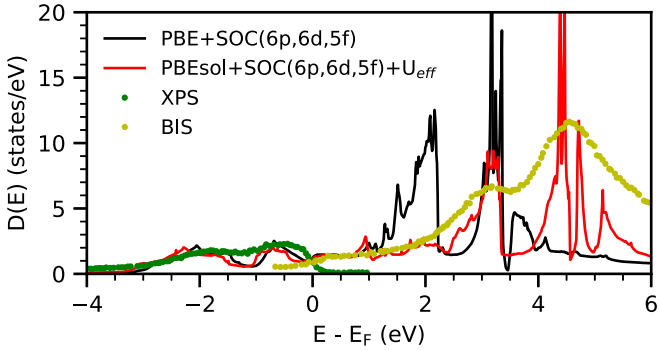

FIG. 2. The total electron density of states $D(E)$ of fcc Th for two different exchange and correlation potentials presented together with the BIS and XPS measurements [30].

B. Elastic properties of thorium metal

Concerning mechanical properties of Th, several theoretical works have been conducted [34–40] with different methods and treatment of electron exchange and correlation effects, but none of them can reproduce all elastic constants and especially problematic c_{12}. Only a few authors [34,35] take into account the spin-orbit coupling.

There are three elastic constants, namely c_{11}, c_{12}, and c_{44}, in a cubic crystal structure. Our results are presented in Table I and compared to the ones obtained with other theoretical and experimental studies for fcc thorium. All previous theoretical calculations [34–40] fail to fully reproduce all elastic constants at the same time, mainly c_{12}, which is in most calculations significantly underestimated.

Although the inclusion of the SOC($6p, 6d, 5f$) increases the problematic c_{12}, simultaneously it also increases c_{44} further away from experimental values. The elastic constant c_{11} is overestimated, but closer to the experiment [32,33] than without the SOC($6p, 6d, 5f$).

In summary, the inclusion of the SOC for the $6p$ states of thorium has a significant impact on the elastic constants. The inaccurate description of the $6p_{1/2}$ can be the decisive reason why the theoretical works are not able to fully reproduce all elastic constants concurrently. The supporting argument is based on an increase of the bulk modulus from 54.5 GPa to 58.3 GPa when the fully relativistic scheme is used [24]. The reported value is very close to the experimental values 58 GPa and 60 GPa [32,33].

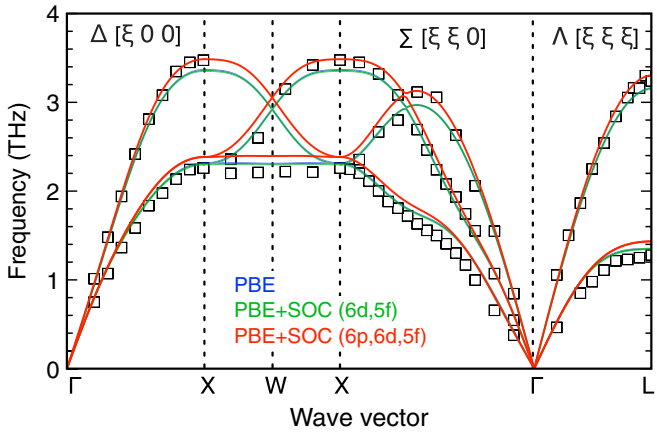

FIG. 3. The dispersion relations of fcc Th phonons. The blue line represents PBE, the green line represents PBE + SOC($6d, 5f$), the red line represents PBE + SOC($6p, 6d, 5f$), and the black squares are the experimental data [41].

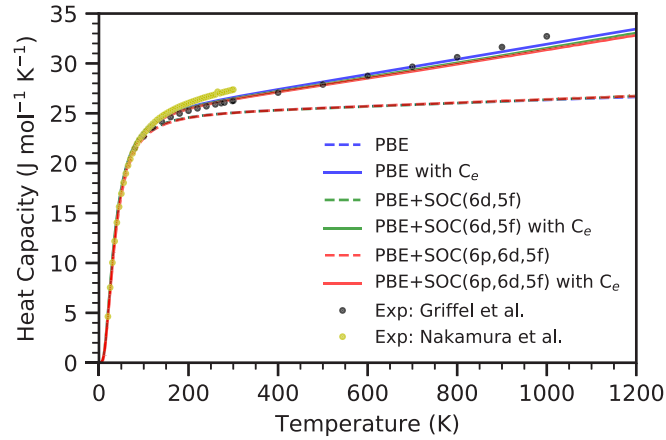

FIG. 4. The heat capacities of Th at constant pressure as a function of temperature. The experimental values are from Griffel *et al.* [42] (black circles) and Nakamura *et al.* [43] (yellow circles).

The elastic constants of PBE + SOC($6d, 5f$) support the previous statement that the SOC for $6d$ and $5f$ states has only a minor effect on the system and can be neglected.

Although only the PBEsol exchange and correlation potential gives excellent agreement with the BIS measurement, it fails to reproduce the experimental elastic coefficients and bulk modulus for all Hubbard U values (Table S1 of the Supplemental Material [31]).

The model (PBEsol + SOC + $U_{\text{eff}} = 4$ eV) that successfully reproduces XPS and BIS experiments overestimates c_{44} and underestimates c_{12} from an excessive occupation of the $6d$ states at the expense of the $5f$ states. It clearly shows that in the PBE + SOC($6p, 6d, 5f$) model the $6d$ states are underestimated (low c_{12}) and the $5f$ states are overestimated (high c_{44}). It may or may not be an indirect effect of the poorly described $6p_{1/2}$ states.

C. Lattice dynamics of thorium metal

There is only one unique atom in its primitive cell for fcc thorium. Thus there are only three independent phonon modes in dispersion relations. In Fig. 3, we present the phonon dispersion curves of thorium as calculated along with several symmetry directions for the PBE potential.

The directions $\Delta[\xi\,0\,0]$, $\sum[\xi\,\xi\,0]$, and $\Lambda[\xi\,\xi\,\xi]$ have been carried out at zero temperature with the comparison of the experimental data obtained from the neutron-scattering measurement at ambient conditions [41]. Figure 3 reveals that the shift to higher frequencies from the inclusion of the SOC($6p, 6d, 5f$) is needed to describe dispersion relations of the longitudinal phonon branches correctly. However, at the same time it overestimates the frequency of the transverse phonon branches. This shift probably only comes from the volume change. A similar effect of the SOC was reported in previous theoretical work [27]. In accord with our previous findings, the SOC($6d, 5f$) has minimal impact on the phonon spectrum.

All phonon dispersion relations of thorium reproduce the anomalous behavior of the transverse branches along the $\sum[\xi\,\xi\,0]$ direction even though we did not include the electron-phonon interaction.

We also calculated the phonon spectrum of PBEsol (Fig. S4). Although PBEsol + SOC($6p, 6d, 5f$) + $U_{\text{eff}} = 4$ eV fails to describe elastic properties, it surprisingly gives good agreement with the experimental data of the phonon dispersion curves [41]. The only discrepancy can be found for the longitudinal mode along $\sum[\xi\,\xi\,0]$ close to Γ. A similar shift to higher frequencies is observed because of the inclusion of SOC as in PBE.

Although PBEsol with the Hubbard model reproduces some quantities better than PBE, this trend cannot always be found (see elastic constants). Moreover, such a strong localization is not physical for thorium and is an artificial correction. For this reason, we have decided not to investigate this model further.

The heat capacity of metal consists of two parts: atomic vibrations (phonons) and the electronic contribution. The lattice vibrations dominate for all temperature ranges. The electronic part has an only weak effect on the total heat capacity at low temperature. However, its importance grows with increasing temperature, and it has negligible size at ordinary operating temperatures in a nuclear fuel cycle. High heat capacity for nuclear fuel is required because it serves as protection against overheating and subsequent fuel melting. Thus, metallic materials are more desirable than insulators.

The heat capacities at constant pressure with and without the electronic contribution (C_e), which are depicted in Fig. 4, grow very fast at low temperatures and reach the Dulong-Petit limit of $3R$ valid for heat capacity at a constant volume at 187 K. After rapid growth at low temperatures, linear growth stemmed mainly from the electronic contribution. The phonon heat capacities of thorium are not sensitive to the spin-orbit coupling, which is also visible from almost the same Debye temperatures listed in Table I. The electronic heat capacities slightly differ due to the different value of the electron-phonon coupling parameter for scalar-relativistic ($\lambda = 0.577$) and full-relativistic solutions ($\lambda = 0.456$), as discussed above.

Figure 5 represents the reduced volume of fcc thorium. Unfortunately, no temperature-dependent experimental data

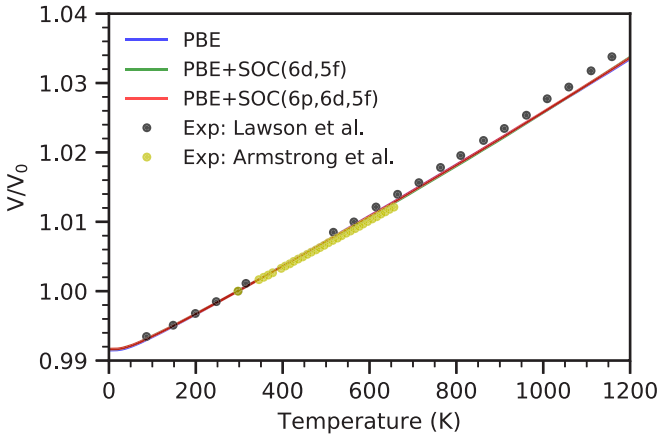

FIG. 5. The reduced volumes $V(T)/V_0$ versus temperature for fcc Th compared to the experimental measurements by Armstrong *et al.* [33] (black circles) and Lawson *et al.* [44] (yellow circles).

of lattice constants are available. The only existing experimental data related to the thermal expansion of thorium are obtained using the V/V_0 relation, where V_0 is the volume at 297 K. Figure 5 demonstrates excellent agreement with both experimental measurements [33,44]. The difference between the model without and with the SOC is not found.

We conclude that the SOC has no significant effect on the thermodynamic properties of thorium.

D. Electronic structure of thorium monocarbide

Figure 6 shows a modification of the electronic structure of ThC upon the SOC. The same trend as with thorium is observed: the inclusion of the SOC to the $6d$ and $5f$ electrons has almost zero effect on the DOS. However, we find a moderate modification of the DOS around the vicinity of the Fermi energy within the inclusion of the SOC to the $6p$ states (indirect effect of the semicore $6p$ states). The peaks of the DOS get sharper than in the scalar-relativistic solution.

Then we analyzed the DOS in the same manner for the PBEsol exchange-correlation potential (Fig. 7), which proved to be successful for uranium monocarbide [45]. There is no significant difference between those exchange-correlation potentials from the electron structure point of view. We also observe almost zero difference with the SOC$(6d, 5f)$ and

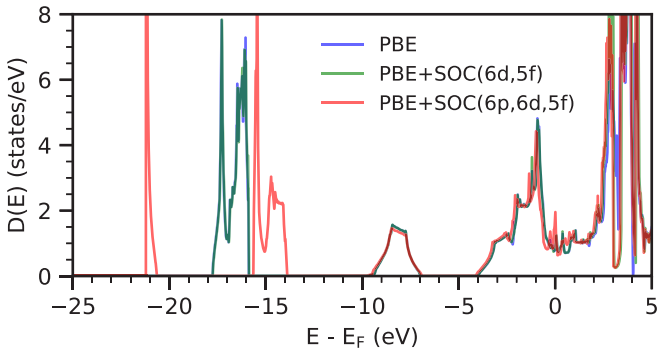

FIG. 6. The total densities of electron states $D(E)$ for ThC calculated with PBE, PBE + SOC$(6d, 5f)$, and PBE + SOC$(6p, 6d, 5f)$.

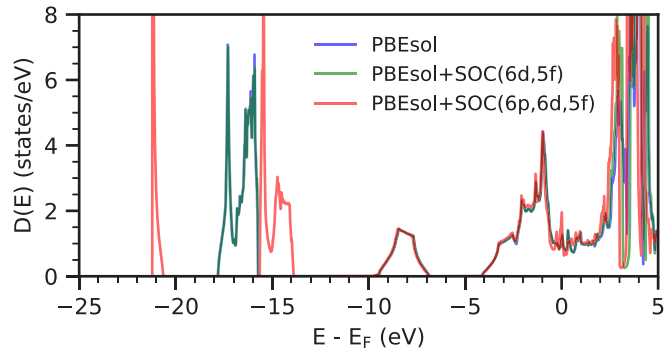

FIG. 7. The total densities of electron states $D(E)$ for ThC calculated with PBEsol, PBEsol + SOC$(6d, 5f)$, and PBEsol + SOC$(6p, 6d, 5f)$.

sharper shape around the Fermi energy with the SOC acting on the $6p$ states. These peaks come from the hybridization of the Th $6d$, Th $5f$, and C $2p$ states, as shown in Fig. 8.

Surprisingly, the SOC$(6p, 6d, 5f)$ does not seem to improve the DOS, but quite the contrary. The Sommerfeld coefficients of both exchange-correlation potentials (PBE/PBEsol) indicate that the more accurate DOS is based on the model without the SOC on the $6p$ states because its values of $2.07/2.76\,\mathrm{mJ\,K^{-2}\,mol^{-1}}$ are much closer to the experimental values $(2.1 - 2.9\,\mathrm{mJ\,K^{-2}\,mol^{-1}})$ [46,47] than $4.51/4.11\,\mathrm{mJ\,K^{-2}\,mol^{-1}}$. The high value of the Sommerfeld coefficient is due to the sharp peak that appears by adding the SOC to the $6p$ states. Moreover, the calculated values do not include the electron-phonon many-body enhancement

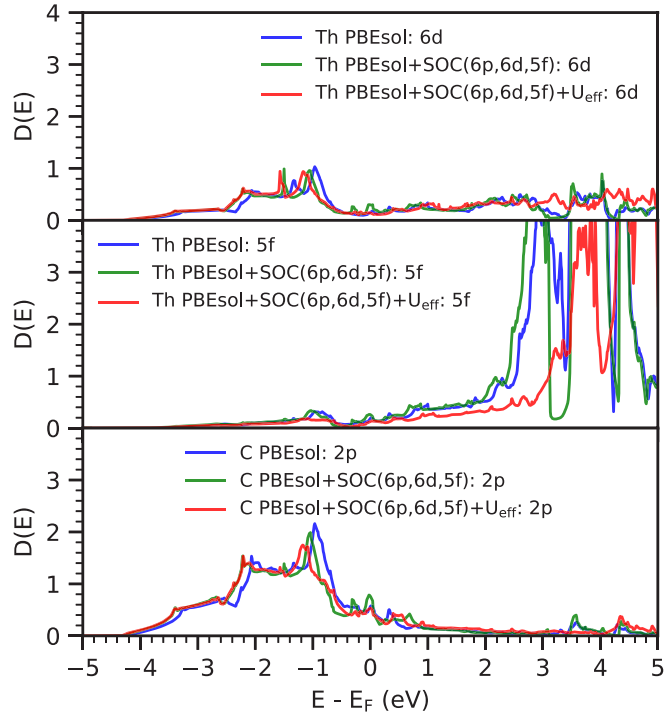

FIG. 8. The projected densities of electron states $D(E)$ for ThC calculated with PBEsol, PBEsol + SOC$(6p, 6d, 5f)$, and PBEsol + SOC$(6p, 6d, 5f)$ with the Hubbard $U_{\mathrm{eff}} = 3\,\mathrm{eV}$.

TABLE II. The calculated and experimental lattice parameters (a), elastic constants c_{ij}, bulk modulus B, Sommerfeld coefficient γ, and Debye temperatures θ_D of NaCl-type ThC.

		E_{xc}	U_{eff} (eV)	a (Å)	c_{11} (GPa)	c_{12} (GPa)	c_{44} (GPa)	B (GPa)	γ (mJ K^{-2} mol^{-1})	θ_D (K)	Reference
ThC	VASP	PBE	0.0	5.354	222.9	93.6	80.1	135.2	2.07	314	This work
	VASP	PBE + SOC($6d, 5f$)	0.0	5.354	225.3	89.4	79.7	134.9	2.06	295	This work
	VASP	PBE + SOC($6p, 6d, 5f$)	0.0	5.335	222.0	86.8	78.5	127.3	4.51	303	This work
	VASP	PBEsol	0.0	5.301	240.0	90.2	78.4	137.3	2.76	335	This work
	VASP	PBEsol + SOC($6d, 5f$)	0.0	5.301	239.4	90.1	78.0	137.3	2.82	334	This work
	VASP	PBEsol + SOC($6p, 6d, 5f$)	0.0	5.279	240.0	87.6	77.0	135.6	4.11	320	This work
	VASP	PBEsol + SOC($6p, 6d, 5f$)	3.0	5.328	264.1	83.2	83.5	144.7	2.46	342	This work
	WIEN2k	PBE	0.0	5.388	252	96	60	148	1.71		Shein [51]
	WIEN2k	PBE+SOC	0.0	5.388	163	70	54	100	2.59		Shein [51]
	CASTEP	PBE	0.0	5.341	276	99	87	158		458	Aydin [52]
	CASTEP	LDA	0.0	5.269	241	96	78	145		478	Aydin [52]
	CASTEP	LDA+U	2.3	5.336	215	88	81	130		470	Aydin [52]
	ESPRESSO	PBE	0.0	5.335	222	86	66	131		298	Daroca [53]
	VASP	PBE	0.0	5.348	216	89	80	137		258	Sahoo [54]
	Exp.			5.335							Street [55]
	Exp.			5.322				109			Gerward [48]
	Exp.			5.340				147			Yu [49]
	Exp.								2.9	280	Harness [46]
	Exp.			5.344					2.1	262	Danan [47]

factor and the theoretical values should be smaller than the experimental values [46,47].

E. Elastic properties of thorium monocarbide

The bulk modulus (B) is the only elastic property that was measured for thorium monocarbide. However, experimental studies are not consistent. Gerward *et al.* [48] report $B =$ 109 GPa while Yu *et al.* [49] $B = 147$ GPa. Olsen *et al.* [50] claim that the discrepancy is possibly due to the difference of stoichiometry. The sample of Yu *et al.* [49] had a composition corresponding to $ThC_{0.95}$ but Gerward *et al.* [48] have a much less stoichiometric $ThC_{0.76}$. The value of 147 GPa is supported by comparison with the lattice parameters and the bulk moduli of thorium nitride (ThN) and thorium sulphide (ThS) [49].

Both PBE and PBEsol predict the bulk modulus approximately to 136 GPa. This is the 7.5% deviation from the experiment [49]. The inclusion of the SOC($6d, 5f$) has only a weak effect for PBE, not PBEsol, as listed in Table II. Decreasing the bulk modulus of PBE is based on decreasing c_{12} but which, however, is partly offset by increasing c_{11}. This is not the case for PBEsol, where all elastic constants slightly decrease.

If we include the SOC also on the $6p$ states, we can observe a similar situation. The changes are again more visible for PBE than PBEsol: the bulk modulus changes from 135 GPa to 127 GPa, in contrast with much a smaller change from 137.3 GPa to 135.6 GPa for the latter one. Nevertheless, it gives worse agreement with an experimental value of 147 GPa in both cases. Other theoretical works (Table II) are not uniform in this matter.

Decreasing of the bulk modulus/elastic constants with smaller volume is in direct contrast to thorium, where we report the opposite effect. It shows that chemical bonding of ThC is much more complex due to the carbon presence.

F. Phonon DOS of thorium monocarbide

Actinide monocarbides are systems with two elements with significantly different atomic mass. Carbon is approximately 20 times lighter than an actinide element. As a result, a phonon spectrum is divided into low-frequency phonons (acoustic branches) arising mainly from oscillations of heavy actinide atoms, and high-frequency phonons (optical branches) arising from oscillations of light carbon atoms. A frequency gap separates these bands.

Figures 9 and 10 present the phonon densities of states for the PBE and PBEsol potentials. While both approaches

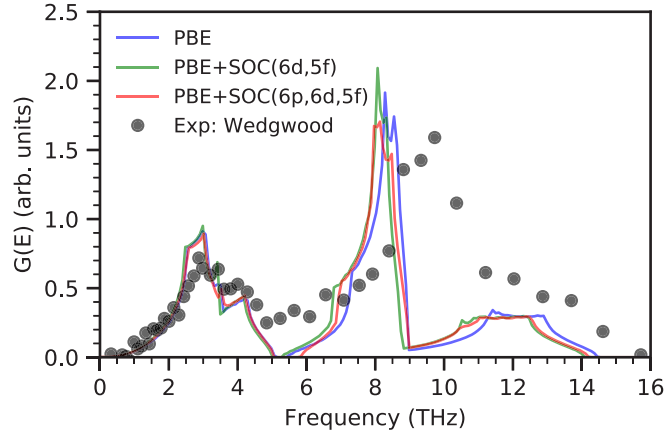

FIG. 9. The phonon densities of states $G(E)$ for NaCl-type structure of ThC. The TOF data (circles) are taken from Wedgwood [56].

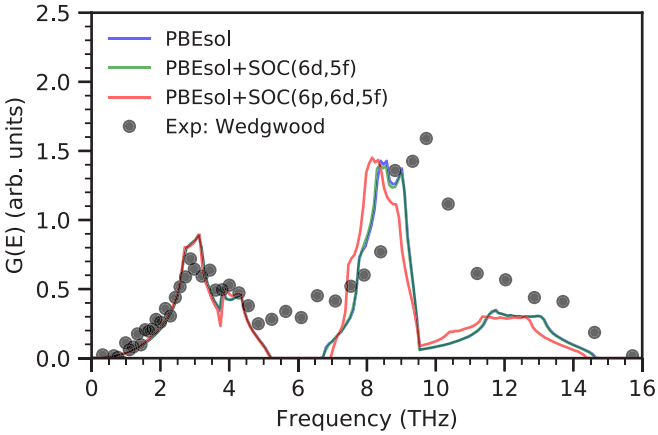

FIG. 10. The phonon densities of states $G(E)$ for NaCl-type structure of ThC. The TOF data (circles) are taken from Wedgwood [56].

describe well the acoustic phonon modes, the comparison of phonon spectra with experiment measured by the time-of-flight (TOF) technique [56] shows that both greatly underestimate the optical phonon modes.

Similarly, an underestimated carbon phonon spectrum of PBE is reported by Daroca *et al.* [53] and Sahoo *et al.* [54]. Their intensity peaks of the optical branches are not consistent with the experimental one [56].

The poor agreement with the experiment suggests that thorium and carbide bonding is much stronger than our models predict. It is consistent with the more than 7% bulk modulus mismatch.

G. Thorium monocarbide with the Hubbard model

The same failure of the PBE approximation to reproduce the optical branches is also well known for uranium monocarbide [45]. The authors solved this inconsistency with the experiment by including the SOC($6p$, $6d$, $5f$) and the Hubbard model.

It is common practice to use the Hubbard model for uranium because uranium consists of $5f^3$ electrons which are partly correlated. However, it is unusual to use the Hubbard model for thorium, because of weak occupancy of the $5f$ states.

We applied the Hubbard model to PBEsol and not on PBE because PBEsol underestimates the lattice parameter and PBE already overestimates. The correct value of the volume is crucial for lattice dynamics.

Unlike uranium where the Hubbard model separates the $5f_{1/2}$ and $5f_{3/2}$ states, including the Hubbard model to thorium only shifts the $5f$ states to higher energies, as shown in Fig. 8. Thus, the occupation of the $6d$ states, which hybridizes better with the $2p$ states and increases the strength of the chemical bond, is raised. Table II shows that the bulk modulus increases to 145 GPa if we apply the Hubbard model with $U_{\text{eff}} = 3\,\text{eV}$. The choice of $U_{\text{eff}} = 3\,\text{eV}$ is based on fitting the experimental lattice parameter (the lattice parameter as a function of the Hubbard U is shown in Fig. S3). The predicted bulk modulus of 145 GPa is very close to the experimental 147 GPa [49].

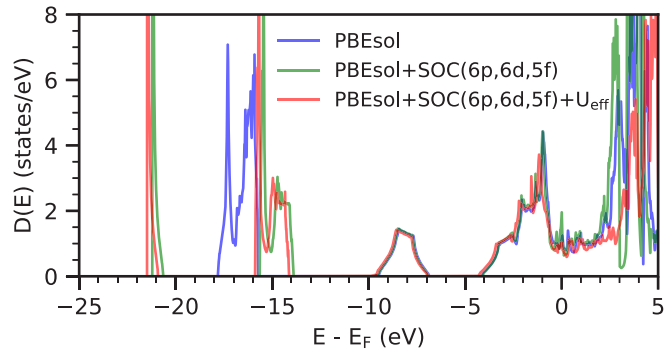

FIG. 11. The total densities of electron states $D(E)$ for ThC calculated with PBEsol, PBEsol + SOC($6p$, $6d$, $5f$), and PBEsol + SOC($6p$, $6d$, $5f$) with Hubbard $U_{\text{eff}} = 3\,\text{eV}$.

While the $5f$ states are shifted to higher energies, all other states are shifted to lower energy, as shown in Fig. 8. It is good correction for the $6p_{1/2}$ states which should be in the lower energies as discussed above, but the $6p_{3/2}$ are incorrectly moved into lower energies, as shown in Fig. 11. It demonstrates that this treatment is artificial.

However, we find much better agreement with the experiment for the Sommerfeld coefficient because the sharp peaks at the vicinity of Fermi energy get flattened. The value $2.46\,\text{mJ}\,\text{K}^{-2}\,\text{mol}^{-1}$ is much closer to $2.1/2.9\,\text{mJ}\,\text{K}^{-2}\,\text{mol}^{-1}$ [46,47] than $4.11\,\text{mJ}\,\text{K}^{-2}\,\text{mol}^{-1}$ when no electron-phonon enhancement is applied.

Furthermore, we find very reasonable agreement with the experimental phonon density of states, as shown in Fig. 12. Not only do we find a perfect match at the optical frequencies, but also the acoustic ones are slightly better. Figure 13 provides the closer look at the phonon dispersion relations which are along the same directions as in thorium metal. The biggest difference can be found in the direction $\Delta[\xi\,0\,0]$ whereas the phonon dispersion curves at the $\Lambda[\xi\,\xi\,\xi]$ direction are much less affected. It follows that greater occupation of the $6d$ states enhances directional chemical bonding.

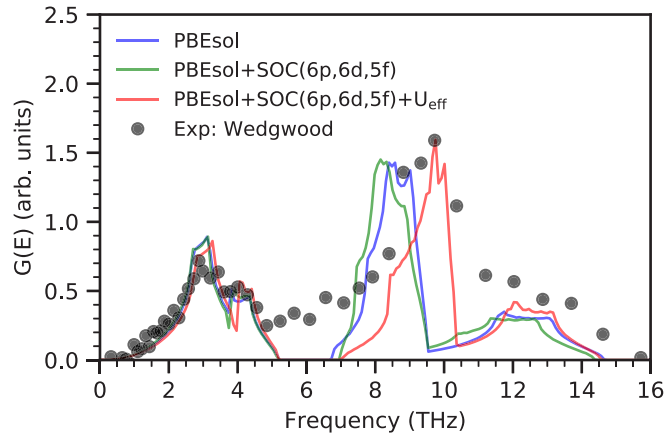

FIG. 12. The phonon densities of states $G(E)$ for NaCl-type structure of ThC. The TOF data (circles) are taken from Wedgwood [56].

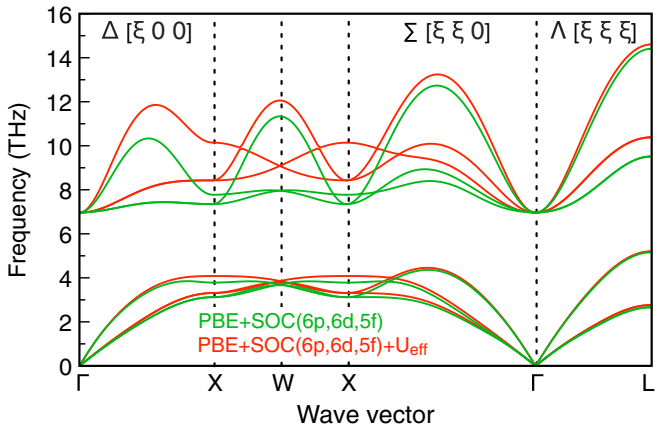

FIG. 13. The phonon dispersion relations of NaCl-type ThC phonons. The blue line represents PBE + SOC($6p$, $6d$, $5f$) and the red line represents PBE + SOC($6p$, $6d$, $5f$) with Hubbard $U_{\text{eff}} = 3$ eV.

We conclude that the correct treatment of the spin-orbit coupling acting on the $6p$ states or special treatment of the $5f$ states is needed even for thorium compounds and simple DFT cannot be used.

H. Thermodynamic properties of thorium monocarbide

Thermodynamics properties are the most important properties for the design of nuclear fuels. Above all, these are heat capacity, thermal expansion, and thermal conductivity. Thermal conductivity is discussed in detail in the next chapter.

Figure 14 illustrates the heat capacities for PBE, PBE + SOC($6p$, $6d$, $5f$), and PBE + SOC($6p$, $6d$, $5f$) + U_{eff}(3 eV) at constant pressure. Both models without the Hubbard model overestimate the experimental measurement [47]. The same problem is reported by Daroca *et al.* [53] and Sahoo *et al.* [54]. Only if the optical frequencies are described well do we get an excellent agreement with the experiment [47]. The slower growth of the heat capacity is caused by insufficient thermal energy to excite the high phonon frequencies, which

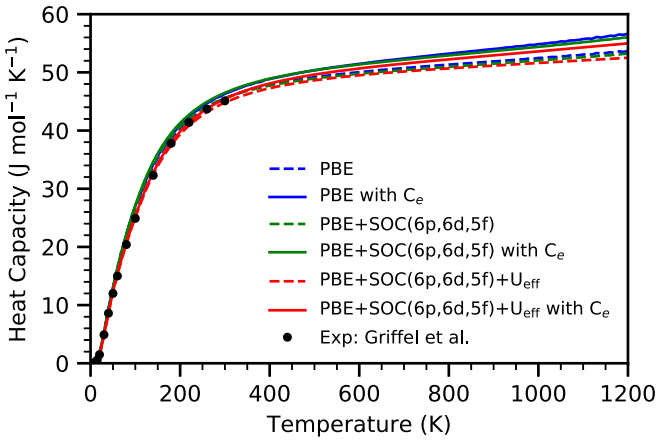

FIG. 14. The calculated heat capacities at constant pressure as a function of temperature for ThC. The experimental values of ThC are from Danan [47] (black circles).

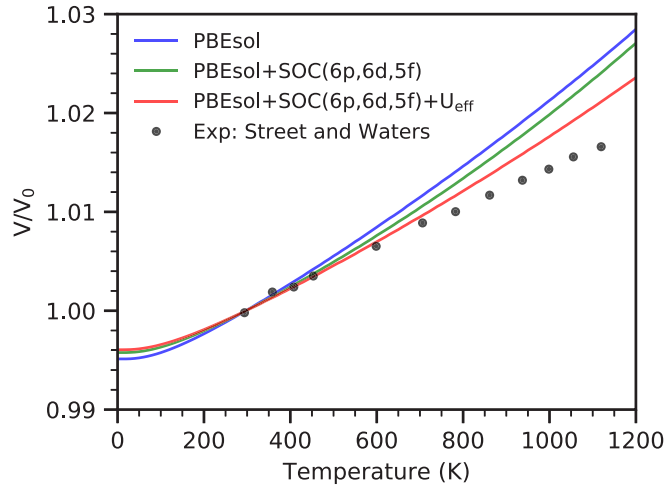

FIG. 15. The reduced volume $V(T)/V_0$ versus temperature for ThC. The experimental data (black circles) are adopted from Street and Waters [55].

again emphasizes the correct description of the optical phonon branches.

The electronic heat capacities are approximately 3–4 times lower per atom in comparison with the elemental metal due to a decrease of metallic bonding in monocarbides.

Next, we present the reduced volume of thorium monocarbide in the same manner as with thorium, in Fig. 15. The V/V_0 ratio, where V_0 is the volume at 297 K, gives us a comparison independent of the initial value while allowing us a direct comparison with thorium.

The reduced volume of PBE does not fit the experiment [55] at all. Inclusion of the SOC($6p$, $6d$, $5f$) improves the agreement with experiment, but a reasonable match can only be found in the PBE + SOC($6p$, $6d$, $5f$) + U_{eff}(3 eV) model. The comparison between the theoretical and experimental reduction of the volume of thorium monocarbide indicates that the influence of high-order anharmonicity on the thermodynamic properties becomes more prominent around 800 K.

The comparison of Figs. 5 and 15 shows the huge difference between the reduced volume of thorium metal and thorium monocarbide. Thorium monocarbide expands around 50% less than thorium due to much stronger chemical bonding.

We conclude that the SOC($6p$, $6d$, $5f$) has a weak effect on the thermodynamic properties of thorium monocarbide and the Hubbard model is needed for perfect agreement with the experiments.

I. Thermal conductivity of thorium metal

Thermal conductivity is the most important property of nuclear fuel because it influences all process such as swelling, grain growth, and fission gas release and limits linear power [60]. For the design of new nuclear materials, it is necessary to provide a method that can predict this material property under different conditions (stoichiometry, nonstoichiometry, gas bubbles, etc.). In this work, we focus on calculating the thermal conductivity of the stoichiometric composition.

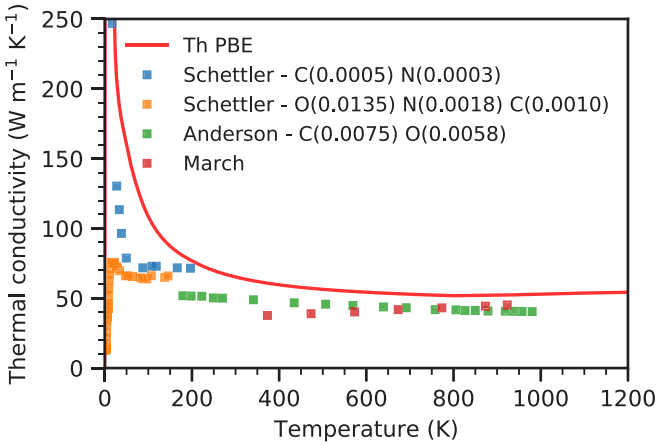

FIG. 16. The total thermal conductivity of fcc Th. The experimental values are from Schettler *et al.* [57] (blue and orange), Anderson *et al.* [58] (green), and March *et al.* [59] (red).

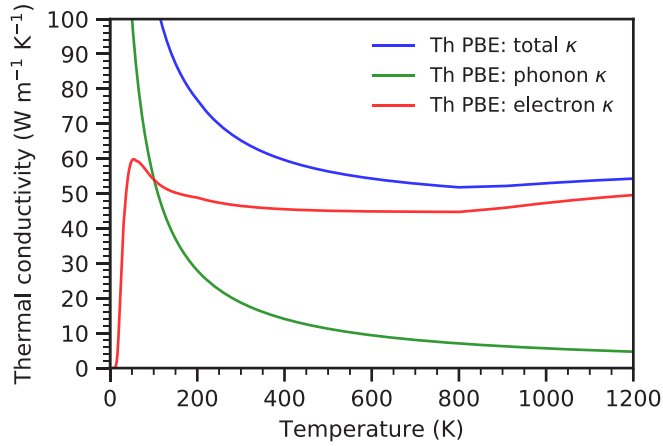

FIG. 17. The phonon and electron parts of the thermal conductivity of Th (PBE).

Thermal conductivity of metal is composed of two components: phonon and electronic thermal conductivity. The electronic part of thermal conductivity causes that metals have mostly several times higher thermal conductivity at high temperatures than isolators, which are commonly used in nuclear power.

We chose the PBE model without the SOC for detailed analysis of the thermal conductivity because the importance of the SOC on lattice dynamics has not been demonstrated. The comparison of our theoretical results and experimental data [57–59] of total thermal conductivity of thorium metal is depicted in Fig. 16 and shows that our calculations are in good agreement with the experiments at higher temperatures, which are more relevant to the actual operating conditions of fuels.

Understandably, our results overestimate the experimental results in the low-temperature region because our model crystal is fully stoichiometric without defects and experimental samples are not. It is needed to modify total phonon lifetimes according to the equation

$$\frac{1}{\tau} = \frac{1}{\tau_{\text{pd}}} + \frac{1}{\tau_{\text{ld}}} + \frac{1}{\tau_{\text{gb}}} + \frac{1}{\tau_{\text{vd}}} + \frac{1}{\tau_{\text{ph-ph}}} \tag{17}$$

to simulate real crystals. The phonon lifetimes τ_{pd}, τ_{ld}, τ_{gb}, τ_{vd}, and $\tau_{\text{ph-ph}}$ correspond to the phonon scattering by point defects (substitutional atoms, interstitials, vacancies, isotopic defects), line defects, grain boundaries, volume defects, and anharmonicities. The scattering cross section has a different dependance on the phonon wavelength (λ) for each of the defects. The cross section for a point defect varies as $1/\lambda^4$, $1/\lambda^3$ for line defects, $1/\lambda^2$ for the grain boundary, and $1/\lambda$ for volume defects [61].

The exact composition of the samples from Schettler *et al.* [57] are $Th_{0.9992}C_{0.0005}N_{0.0003}$ and $Th_{0.9847}C_{0.0135}N_{0.0018}$ and the sample from Anderson *et al.* [58] is $Th_{0.9867}C_{0.0075}N_{0.0058}$. The composition of the March *et al.* [59] sample is unknown.

Figure 18 presents the total thermal conductivity of thorium monocarbide and the contributions of the phonon and electron parts.

The maximum of the phonon thermal conductivity of thorium can be found below 20 K. The intensity of the peak strongly depends on the purity of a sample. Schettler *et al.* [57] measured two samples of different impurity ratios, and the intensity of the more stoichiometric sample was up to 7 times higher. Our results are based on the stoichiometric crystal, so our calculation greatly overestimates the maximum of the experimental phonon thermal conductivity. This inconsistency with the experiment disappears around 200 K when umklapp scattering prevails over normal scattering.

The course of the electronic thermal conductivity is different from the phonon thermal conductivity. It rises sharply as electrons begin to acquire energy required for excitation into the conduction bands while the lattice vibrates with small magnitude. The relaxation times of electrons for each temperature, which we calculated from the experimental resistivity measurements [62,63], take high values at low temperature (10^{-13} s) and sharply decline once the phonon-electron interactions start to play a role (10^{-15} s). After the peak of the electronic thermal conductivity around 40 K, there is a slight decrease and then almost a constant value, while the phonon contribution is still decreasing exponentially.

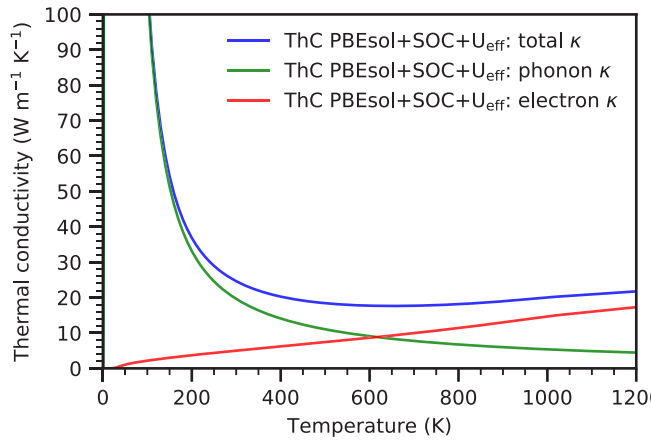

FIG. 18. The phonon and electron parts of the thermal conductivity of ThC (PBE + SOC + $U_{\text{eff}} = 3$ eV).

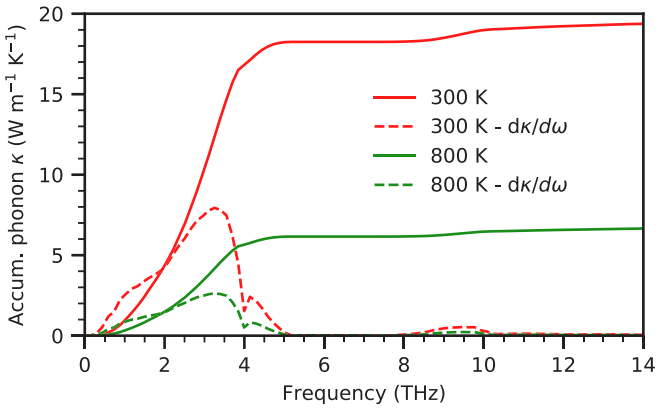

FIG. 19. The accumulated phonon thermal conductivity as a function of the phonon frequency of ThC.

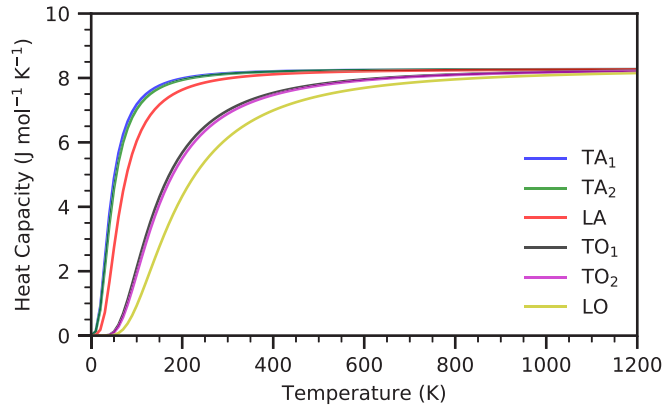

FIG. 21. The heat capacity per mode of ThC as a function of temperature.

In general, the thermal conductivity of thorium is controlled primarily by the phonon part to the temperature around 60 K, where both parts are equal. From this temperature, the electronic contributions begin to dominate over phonon ones, and for even higher temperature, one can neglect phonons.

J. Thermal conductivity of thorium monocarbide

We use the PBE + SOC($6p, 6d, 5f$) + U(3 eV) model for the thermal conductivity calculations of thorium monocarbide, because it is the only model which correctly describes the lattice dynamics properties.

There is a considerable difference in the thermal conductivity between thorium metal and thorium monocarbide. This is apparent from the comparison of Figs. 17 and 18. The total thermal conductivity of thorium monocarbide is more than twice as small as thorium metal. This difference is based on the lesser electron part of the thermal conductivity (the relaxation times of conductive electrons were also derived from experimental resistivity measurements [64,65]). This is consistent with the twice smaller value of the Sommerfeld coefficient and generally much weaker metallic behavior of thorium monocarbide. The opposite trend can be observed at the phonon part where the phonon thermal conductivity of thorium monocarbide is slightly larger than in thorium metal.

To analyze the phonon thermal conductivity of thorium monocarbide, the accumulated thermal conductivities at 300 K and 800 K and their derivatives with respect to the energy are plotted in Fig. 19. The acoustic branches contribute to 94% of the phonon thermal conductivity. This result differs significantly from NpO_2 when the optical branches contribute to 27% of the phonon thermal conductivity [66].

The optical branches of thorium monocarbide do not contribute significantly in the whole temperature range, as shown in Fig. 20.

The phonon thermal conductivity is a function of the heat capacity, group velocity, and phonon lifetime of phonon mode, as shown in Eq. (5). There is a difference between the heat capacities for the acoustic and optical branches. One can see in Fig. 21 that the difference disappears at higher temperature where Bose-Einstein statistics go into classical Maxwell-Boltzmann statistics. There is also the difference between the transverse and longitudinal branches where the former ones have higher heat capacity per mode at a lower temperature due to smaller vibrational frequencies. Nevertheless, the heat capacity does not seem to be a determining factor as the heat capacities of the optical modes are almost the same as the acoustic modes at 800 K; see Fig. 19.

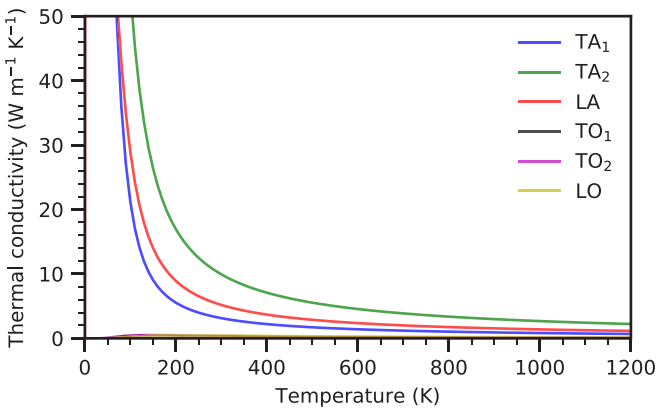

FIG. 20. The phonon part of the thermal conductivity of ThC per mode as a function of temperature.

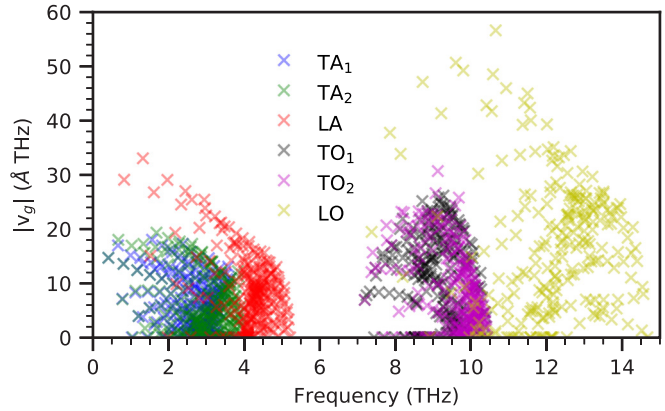

FIG. 22. The absolute value of the group velocity of ThC in the xx direction as a function of the phonon frequency.

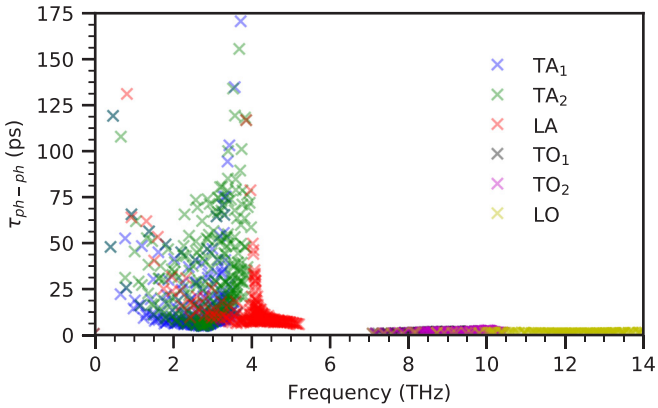

FIG. 23. The phonon lifetime distribution of ThC as a function of the phonon frequency.

Next, we discuss the group velocity in the xx direction, as displayed in Fig. 22. The optical modes have about twice the average group velocity of the acoustic ones. The most significant difference can be found at the longitudinal optical mode because the mode is very dispersed (see Fig. 13).

Although the group velocities of the optical branches are higher, the optical branches contribute to the total phonon conductivity only a little. This brings us to the final variable: phonon lifetime. Figure 23 gives us an explanation of why the optical phonon branches almost do not transfer heat. The phonon lifetimes of the optical modes are more than 25 times smaller than the lifetimes of the acoustic modes. The scattering of the optical phonon is vast, and therefore, these modes cannot effectively transfer energy (heat).

It is also worth mentioning an explanation of why the transverse acoustic mode (TA_2) has a greater contribution to the total phonon conductivity than the longitudinal acoustic mode (LA), as shown in Fig. 20. We found the same explanation as for the previous discussion. Though the average group velocity of the transverse mode is around 30% smaller than the longitudinal one, the average phonon lifetime of the transverse acoustic mode (TA_2) is 3 times greater than the longitudinal acoustic mode (LA).

V. CONCLUSIONS

The electronic, elastic, phonon, and thermodynamic properties of fcc thorium and thorium monocarbide (rocksalt structure) have been explored within the inclusion of the spin-orbit coupling with the use of density functional theory calculations.

Although the spin-orbit coupling does not influence the distribution of the density of states at the vicinity of the Fermi energy, which is formed mainly by the $6d$ and $5f$ states, significant splitting of the $6p$ states is observed.

The analysis of elastic constants suggests that it is necessary to increase the occupation of the $6d$ states at the expense of the $5f$ states to reproduce the experimental elastic properties. The incorrect description of the $6p_{1/2}$ states caused by not using a relativistic basis may be the cause of undervalued theoretical c_{12} and overvalued c_{44} elastic constants.

The changes resulting from the addition of the SOC to the $6d$ states and the $5f$ states are negligible. Only the SOC acting on the $6p$ states can be important for some properties. Nevertheless, for thermodynamic properties, the importance of the SOC has not been proved and may be neglected in the theoretical calculations for thorium.

The situation is quite different for ThC. The density of states at the vicinity of the Fermi energy is modified by including the SOC on the $6p$ states. It yields a worse value of the Sommerfeld coefficient in comparison with the experiments. The same deterioration can be found for the bulk modulus. However, the importance of the SOC acting on the $6d$ states and the $5f$ states is also not found like for thorium.

The breaking point is the analysis of the phonon density of states. We are not able to reproduce the optical phonon branches with or without the SOC. The same problem was found in uranium monocarbide. The mismatch is more than 1.5 THz. The only solution to get an agreement with experiment is adding the Hubbard model which acts on the $5f$ states.

This is an unconventional solution because thorium has very few occupied $5f$ states, and there is no physical sense of increasing on-site Coulomb repulsion. It is more of an artificial correction. However, this correction gives us an excellent agreement with the experimental phonon DOS. We also find a better match for the heat capacity and reduced volume.

Since we cannot describe the thorium compound dynamics by a simple DFT with the second variational approach, this raises the question of whether the precise description of the $6p$ states is needed or the description of the $5f$ electrons is insufficient even at such a low occupation. This will be investigated in the near future because it can be important for more early actinide compounds in general.

As for comparisons of elemental thorium and thorium monocarbide, thermodynamic properties of ThC are significantly affected by the changes in chemical bonding. Ionic and covalent ones in ThC largely replace metal bonding. This causes slower growth of the heat capacity (phonon part) at the lower temperature range, and the electron part of ThC heat capacity is approximately 3–4 times lower per atom than in Th. The stronger bonding also causes much less thermal expansion than in thorium.

The total thermal conductivity was determined for both materials. We conclude that our phonon and electronic parts of thermal conductivity are well described because the calculated total thermal conductivity of thorium is in good agreement with the experimental values.

The total thermal conductivity varies considerably between Th and ThC. The total thermal conductivity of thorium is more than twice as large as that of ThC due to the much larger electron part of the thermal conductivity. The electronic part of the thermal conductivity of ThC is smaller due to fewer conducting electrons.

From the detailed analysis of the phonon thermal conductivity of ThC, it is shown that the acoustic branches contribute 94% of the phonon thermal conductivity because the optical phonon modes have small lifetimes. We do not find the importance of the optical branches as with NpO_2 where the optical branches contribute 27% of the phonon thermal conductivity. Despite all this, ThC has the higher phonon thermal conductivity than NpO_2, and this shows the importance of the acoustic branches.

ACKNOWLEDGMENTS

This work was supported by the European Regional Development Fund Supercomputing Center, Path to Exascale project, Project No. CZ.02.1.01/0.0/0.0/16_013/0001791, within the Operational Programme Research, Development, and Education, by Grant No. 17-27790S of the Czech Science Foundations, and by the Ministry of Education, Youth, and Sports, Mobility Grant No. 8J18DE004.

[1] J. D. Greiner and J. F. Smith, Phys. Rev. B **4**, 3275 (1971).

[2] Edited by L. Manes, *Actinides: Chemistry and Physical Properties* (Springer, Berlin, 1985).

[3] B. Johansson, R. Ahuja, O. Eriksson, and J. M. Wills, Phys. Rev. Lett. **75**, 3968 (1995).

[4] L. R. Morss, N. M. Edelstein, and J. Fuger (eds.), *The Chemistry of the Actinide and Transactinide Elements* (Springer, Dordrecht, 2010).

[5] T. Abram and S. Ion, Energy Policy **36**, 4323 (2008).

[6] IAEA, *Thorium Fuel Cycle: Potential Benefits and Challenges*, IAEA TECDOC Series No. 1450 (International Atomic Energy Agency, Vienna, 2005).

[7] J. Mulak, W. Suski, and R. Troć, in *2nd International Conference on the Electronic Structure of the Actinides, 13–16 September 1976, Wroclaw* (Zakład Narodowy im. Ossolińskich, Wrocław, 1976).

[8] A. Togo, L. Chaput, and I. Tanaka, Phys. Rev. B **91**, 094306 (2015).

[9] G. K. Madsen, J. Carrete, and M. J. Verstraete, Comput. Phys. Commun. **231**, 140 (2018).

[10] J. Ziman, *Electrons and Phonons* (Oxford University Press, Oxford, 2001).

[11] C. Wolverton and A. Zunger, Phys. Rev. B **52**, 8813 (1995).

[12] G. Kresse and J. Furthmüller, Phys. Rev. B **54**, 11169 (1996).

[13] P. E. Blöchl, Phys. Rev. B **50**, 17953 (1994).

[14] G. Kresse and D. Joubert, Phys. Rev. B **59**, 1758 (1999).

[15] J. P. Perdew, K. Burke, and M. Ernzerhof, Phys. Rev. Lett. **77**, 3865 (1996).

[16] J. P. Perdew, A. Ruzsinszky, G. I. Csonka, O. A. Vydrov, G. E. Scuseria, L. A. Constantin, X. Zhou, and K. Burke, Phys. Rev. Lett. **100**, 136406 (2008).

[17] A. I. Liechtenstein, V. I. Anisimov, and J. Zaanen, Phys. Rev. B **52**, R5467 (1995).

[18] D. van der Marel and G. A. Sawatzky, Phys. Rev. B **37**, 10674 (1988).

[19] A. Togo and I. Tanaka, Scr. Mater. **108**, 1 (2015).

[20] P. Vinet, J. Ferrante, J. H. Rose, and J. R. Smith, J. Geophys. Res. **92**, 9319 (1987).

[21] Y. L. Page and P. Saxe, Phys. Rev. B **65**, 104104 (2002).

[22] L. Nordström, J. M. Wills, P. H. Andersson, P. Söderlind, and O. Eriksson, Phys. Rev. B **63**, 035103 (2000).

[23] J. Kuneš, P. Novák, R. Schmid, P. Blaha, and K. Schwarz, Phys. Rev. B **64**, 153102 (2001).

[24] A. E. Mattsson and J. M. Wills, Int. J. Quantum Chem. **116**, 834 (2016).

[25] H.-G. Schmidt and G. Wolf, Solid State Commun. **16**, 1085 (1975).

[26] J. E. Gordon, H. Montgomery, R. J. Noer, G. R. Pickett, and R. Tobón, Phys. Rev. **152**, 432 (1966).

[27] P. González-Castelazo, R. de Coss-Martínez, O. D. la Peña-Seaman, R. Heid, and K.-P. Bohnen, Phys. Rev. B **93**, 104512 (2016).

[28] H. L. Skriver and I. Mertig, Phys. Rev. B **32**, 4431 (1985).

[29] H. L. Skriver, O. Eriksson, I. Mertig, and E. Mrosan, Phys. Rev. B **37**, 1706 (1988).

[30] Y. Baer and J. K. Lang, Phys. Rev. B **21**, 2060 (1980).

[31] See Supplemental Material at http://link.aps.org/supplemental/10.1103/PhysRevB.101.075117 for the DOS, elastic constants, lattice parameter, and phonon dispersion including/excluding spin-orbit coupling for semicore and valence states as well as the inclusion of the Hubbard U for the PBEsol exchange-correlation functional.

[32] J. D. Greiner, D. T. Peterson, and J. F. Smith, J. Appl. Phys. **48**, 3357 (1977).

[33] P. E. Armstrong, O. N. Carlson, and J. F. Smith, J. Appl. Phys. **30**, 36 (1959).

[34] P. Söderlind, O. Eriksson, J. M. Wills, and A. M. Boring, Phys. Rev. B **48**, 9306 (1993).

[35] P. Söderlind, O. Eriksson, B. Johansson, and J. M. Wills, Phys. Rev. B **52**, 13169 (1995).

[36] J. Bouchet and R. C. Albers, J. Phys.: Condens. Matter **23**, 215402 (2011).

[37] S. C. Gupta, K. Joshi, and S. Banerjee, Metall. Mater. Trans. A **39**, 1593 (2007).

[38] J. Baria and A. Jani, Phys. B (Amsterdam) **405**, 2065 (2010).

[39] C.-E. Hu, Z.-Y. Zeng, L. Zhang, X.-R. Chen, and L.-C. Cai, Solid State Commun. **150**, 393 (2010).

[40] S. Jaroszewicz, H. Mosca, and J. Garcés, J. Nucl. Mater. **429**, 136 (2012).

[41] R. A. Reese, S. K. Sinha, and D. T. Peterson, Phys. Rev. B **8**, 1332 (1973).

[42] M. Griffel and R. E. Skochdopole, J. Am. Chem. Soc. **75**, 5250 (1953).

[43] J. Nakamura, Y. Takahashi, S. Izumi, and M. Kanno, J. Nucl. Mater. **88**, 64 (1980).

[44] A. C. Lawson, B. M. Artinez, J. A. Roberts, B. I. Bennett, and J. W. Richardson, Philos. Mag. B **80**, 53 (2000).

[45] U. D. Wdowik, P. Piekarz, D. Legut, and G. Jagło, Phys. Rev. B **94**, 054303 (2016).

[46] J. B. Harness, J. C. Matthews, and N. Morton, Br. J. Appl. Phys. **15**, 963 (1964).

[47] J. Danan, J. Nucl. Mater. **57**, 280 (1975).

[48] L. Gerward, J. Olsen, U. Benedict, and H. Luo, J. Less-Common Met. **161**, L11 (1990).

[49] C. Yu, J. Lin, P. Huai, Y. Guo, X. Ke, X. Yu, K. Yang, N. Li, W. Yang, B. Sun, R. Xie, and H. Xu, Sci. Rep. **7**, 96 (2017).

[50] J. S. Olsen, S. Steenstrup, L. Gerward, U. Benedict, and J.-P. Itié, Phys. B (Amsterdam) **139-140**, 308 (1986).

[51] I. R. Shein and A. L. Ivanovskiĭ, Phys. Solid State **52**, 2039 (2010).

[52] S. Aydin, A. Tatar, and Y. Ciftci, J. Nucl. Mater. **429**, 55 (2012).

[53] D. P. Daroca, S. Jaroszewicz, A. Llois, and H. Mosca, J. Nucl. Mater. **437**, 135 (2013).

[54] B. D. Sahoo, K. D. Joshi, and S. C. Gupta, J. Appl. Phys. **117**, 185903 (2015).

[55] R. S. Street and T. N. Waters, *The Thermal Expansion of ThC and ThN* (Energy Research Establishment, Harwell, 1962).
[56] F. A. Wedgwood, J. Phys. C **7**, 3203 (1974).
[57] H. G. Schettler, J. J. Martin, F. A. Schmidt, and G. C. Danielson, Phys. Rev. **187**, 801 (1969).
[58] R. L. Anderson, D. H. Grotzky, and W. E. Kienzle, in *9th Conference on Thermal Conductivity*, Rept. CONF-691002 (US Department of Energy, Ames, 1969).
[59] L. L. Marsh and J. R. Keeler, *The Technology of Thorium* (US Atomic Energy Commission, Ohio, 1951).
[60] T. R. G. Kutty, J. Banerjee, and A. Kumar, in *Thoria-Based Nuclear Fuels*, Green Energy and Technology, edited by D. Das and S. Bharadwaj (Springer, London, 2013), pp. 11–70.
[61] G. Grimvall, *Thermophysical Properties of Materials*, Selected Topics in Solid State Physics (North-Holland, Amsterdam, 1999).
[62] P. Sahu, M. Yousuf, and K. G. Rajan, Phys. B (Amsterdam) **160**, 177 (1989).
[63] P. Haen and G. Meaden, Cryogenics **5**, 194 (1965).
[64] A. B. Auskern and S. Aronson, J. Appl. Phys. **38**, 3508 (1967).
[65] P. Chiotti, F. Korbitz, and G. Dooley, J. Nucl. Mater. **23**, 55 (1967).
[66] P. Maldonado, L. Paolasini, P. M. Oppeneer, T. R. Forrest, A. Prodi, N. Magnani, A. Bosak, G. H. Lander, and R. Caciuffo, Phys. Rev. B **93**, 144301 (2016).